Article

Initial Studies of Electron Beams as a means of Modifying Collagen

Robert Apsimon [1,2,†,*], Sadiq Setiniyaz [1,2,†], Rebecca Seviour [3], William Wise [4], Maribel Juarez Hernandez [5] and Edgar Ortiz [5]

[1] Engineering Department, Lancaster University, LA1 4YW, UK
[2] Cockcroft Institute, Daresbury Laboratory, Warrington, WA4 4AD, UK
[3] Ion Beam Centre, University of Huddersfield, HD1 3DH, UK
[4] Institute for Creative Leather Technologies, University of Northampton, NN1 5PH, UK
[5] University of Guanajuato, Leon Campus, Leon, Guanajuato, Mexico
* Correspondence: r.apsimon@lancaster.ac.uk
† These authors contributed equally to this work.

Abstract: We present the initial design studies and specifications for an accelerator and conveyor system to irradiate collagen samples, modifying properties such as the putrescibility and mechanical behaviours in a paradigm shift from existing, widely used technology. We show the integrated design requirements for a magnetic rastering scheme to move the beam position in order to ensure a uniform dose distribution over the full surface of the hide and discuss its dependence on factors such as the size of the hide, the beam current and conveyor speed. We also present initial energy deposition studies using G4BeamLine, in order to determine the numerical beam parameters and angle of incidence needed to ensure a uniform depth-dose distribution throughout the hide thickness.

Keywords: leather; tanning; collagen modification; electrons; accelerator; RF; beams

1. Introduction

Particle accelerators are used for a wide range of applications, such as high energy physics experiments [1–3] which are very high profile, but account for less than 1% of all the particle accelerators in operation. The vast majority of accelerators are used for more subtle applications, but have an enormous impact on everyday life. These accelerators are primarily used for security, medical and industrial applications, such as cargo scanning, cancer therapy and manipulating the physical properties for polymers, such as creating thermosetting plastics. In a world with an increasing demand for green technology and sustainability, particle accelerators have great potential for developing disruptive technologies in this respect. This study focuses on the main industrial use of collagen modification - leather manufacture - but there are other applications that could utilise this technology.

The leather production process consists of multiple stages, many of which require non-benign chemicals and can have a long-term impact on the local environment if not properly treated and disposed of [4–6]. Many countries in the developed world such as USA and EU states [7,8] have stringent regulations to ensure that by-products from the leather production are disposed of with minimal impact on the local environment. In developing countries tanneries often have difficulty in meeting the requirements of the regulations.

Leather manufacture is a global, multi-billion dollar industry that involves numerous steps to transform a skin/hide into a piece of finished leather ready for conversion into a product. The number of steps and chemicals involved vary enormously depending on the end use of the leather, but there are normally common steps involved in all processes; one of which is tanning. The tanning process consists of using tanning agents to create branching between protein chains. This process is qualitatively similar to the cross-linking of polymers, which is readily achieved by mixing polymers with cross-linking agents and irradiating with electron beams.

The use of electron beams for collagen modification and in particular leather tanning has several potential advantages over existing technology. One of the more high profile

Citation: Apsimon R.; Setiniyaz S.; Seviour R.; Wise W.; Juarez Hernandez M.; Ortiz E. Initial studies of electron beams as a means of tanning leather. *Preprints* **2021**, *1*, 0. https://doi.org/

Received:
Accepted:
Published:

components used in leather manufacture is chromium with over 80% of the worlds leather containing it. One key advantage of electron beam (e-beam) tanning is that water consumption and and quantities of tannages used in the tanning process can be substantially reduced, with chromium uptake efficiencies reaching close to 100%; this process also allows for simpler recycling of unused tanning agents. It is also expected that tanning would be able to occur over a wider range of temperatures and pH, while also allowing for the use of novel tanning agents that would typically be too unstable in water or air to bind to the collagen. A patent has been filed for this novel technique [9].

Uniformity of the tanning reaction throughout the cross-section of a skin/hide is crucial for the end product to achieve tight specification parameters set by the original equipment manufacturers (OEMs) as well as meeting legislative restrictions. This requires optimisation of the dose distribution over the surface of the hide as well as to ensure a uniform depth-dose distribution.

As discussed in Section 3, in order to optimise the depth-dose curve, the energy spectrum of the beam and/or the angle of incidence of the beam at the hide surface must be tailored. A simple but costly way to achieve this is to use multiple accelerators with different energies or angles of incidence. A sophisticated but more cost effective approach would be to kick out some bunches from the linac at different energies or to deflect certain bunches by differing amounts with the use of fast kickers and septum magnets [10,11]. A simple, inexpensive but a laborious and slower option is irradiate the hide multiple times with different irritation angles and/or energies. In the last option, the conveyor belt can be designed to tilt the hide to different angles. The conveyor belt would go back and forth with different angles. The irradiation time and thus conveyor belt would be adjusted according to the mix ratio.

This paper presents a theoretical study of the design of the beam rastering scheme, which is required to scan the electron beam over the surface of the hide to ensure a uniform dose distribution over the hide surface. This is presented in Section 2. Section 3 presents simulation results of dose deposition through the thickness of the hide and determines the required beam energy spectrum as well as the required angle of incidence of the beam in order to ensure a uniform depth-dose curve. Hence the overall studies in this paper ensure that the dose deposition throughout the volume of the hide is as uniform as possible.

2. Design considerations

2.1. Orientation of target with respects to the beam

As we discuss in this paper, the dose deposition curve of an electron beam can be altered by either changing the energy of the beam, or by varying the angle of incidence of the electron beam on the target. The simulation studies shown in the next section indicate that qualitatively, varying the energy and the angle of incidence has a similar effect on the dose deposition.

We make no assumptions on the preferred means of varying the dose deposition through the hide, instead we simply present different possibilities that allow different options to be considered in later studies. This section, considers the possibilities for varying the angle of incidence of the electron beam, taking into account the challenges faced.

A whole hide from a fully grown bull is approximately $2 \times 2.5\ m^2$ in size and if the intention is to irradiate the entire hide in one piece, then the electron beam must be scanned over the entire width. When a charged particle travels through a uniform magnetic field orientated perpendicular to the direction of motion, as with a dipole magnet, the particle adopts a circular path, with radius of curvature, ρ. Figure 1 shows a schematic diagram of the geometry of the beam trajectory through the raster scanning magnet to the hide. We define θ as the bending angle, l_{dip} as the dipole length, L_{drift} as the distance between the scanning magnet and the centre of the hide.

Figure 1considers the position, z, to be the apparent point of rotation of the beam. That is to say that we know that before and after the dipole magnet, the electron beam trajectory is a straight line, so rather than considering the true curved path of the trajectory

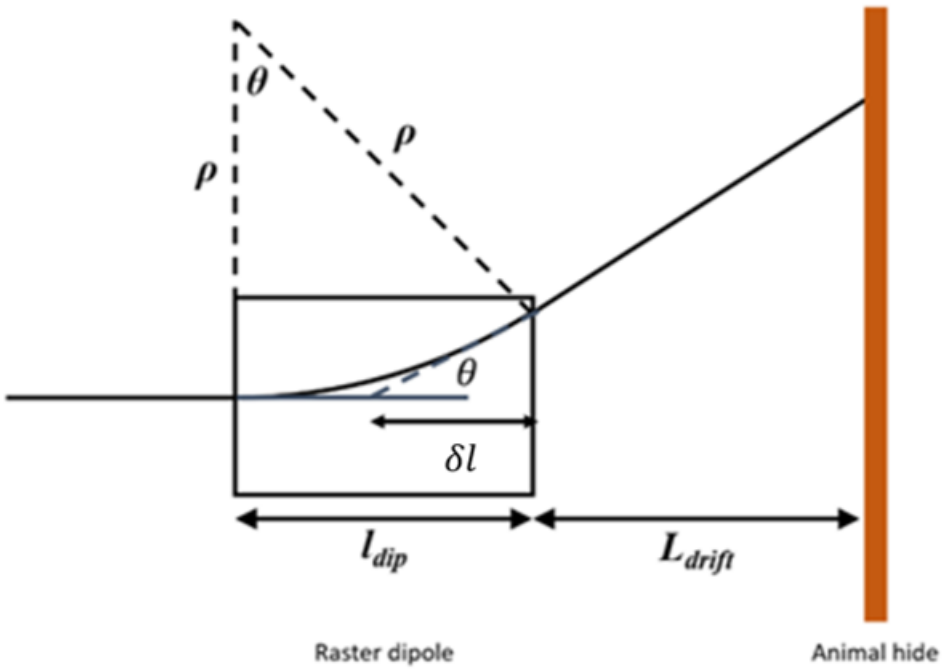

Figure 1. Schematic diagram showing the geometry of the beam trajectory through the raster scanning magnet to the hide.

through the dipole magnet, we can consider that at some location, the beam is rotated by an angle θ. We know that the radius of curvature is given as:

$$\rho = \frac{l_{dip}}{\sin\theta} \tag{1}$$

we also know that the offset of the electron beam at the exit of the raster magnet (where we take $x > 0$ to be to the right of the beam at the entrance of the raster magnet) is given as:

$$x_{off} = \rho(1 - \cos\theta) = l_{dip}\frac{1 - \cos\theta}{\sin\theta}. \tag{2}$$

In terms of θ, the gradient of the line after the raster magnet is given as $\frac{dy}{dx} = tan\theta$, and from this, we obtain:

$$\delta l = \frac{x_{off}}{\tan\theta} = l_{dip}\frac{\cos\theta(1 - \cos\theta)}{\sin^2\theta} = l_{dip}\frac{\cos\theta}{1 + \cos\theta} \tag{3}$$

and from this, if we define the position of the beam at the start of the raster magnet as $(x, y) = (0, 0)$, then the point of rotation is given as $(x, y) = \left(\frac{l_{dip}}{1+cos\theta}, 0\right)$. The point of rotation is not at a fixed position, but rather, it varies with angle, with the position changing more as θ increases.

In order to ensure that we achieve uniform tanning across the hide, we need to ensure that the angle of incidence between the beam and the normal to the surface of the hide is constant across the full scanning range of the beam. It should also be noted that when designing the magnetic rastering scheme, we shall also require that the beam scans over the surface of the hide at a constant rate as well.

We define the angle of incidence of the beam, ϕ, to be the angle between the beam trajectory and the normal to the surface of the hide. For two lines with gradients $m_1 = tan\theta$ and $m_2 = \frac{dy}{dx}$, where the angle of intersect between the lines is $\left(\frac{\pi}{2} - \phi\right)$, then we have:

$$m_1 m_2 + 1 = \sqrt{m_1^2 + 1}\sqrt{m_2^2 + 1}\cos\left(\frac{\pi}{2} - \phi\right), \tag{4}$$

from which we obtain that the gradient of the hide as a function of θ and ϕ as:

$$\frac{dy}{dx} = -\frac{1}{\tan(\theta \pm \phi)}. \tag{5}$$

The choice of sign in Eq. 5 is based on which direction we define angles to be positive. For this paper, we shall choose the positive sign convention, but this is a completely free choice. We also know the equation of the line defining the trajectory of the beam between the raster magnet and the hide must be:

$$y = x\tan\theta - \frac{l_{dip}\sin\theta}{\cos\theta(1+\cos\theta)}. \tag{6}$$

Let us now assume that points (x, y) and $(x + \delta x, y + \delta y)$ are points on the surface of the hide that are sufficiently close together such that we can assume a straight line between them, then from Eq. 5 and 6, we have:

$$\begin{aligned} \delta y &= -\tfrac{\delta x}{\tan(\theta+\phi)} \\ &= (x+\delta x)\tan(\theta+\delta\theta) - \tfrac{l_{dip}\sin(\theta+\delta\theta)}{\cos(\theta+\delta\theta)(1+\cos(\theta+\delta\theta))} - x\tan\theta + \tfrac{l_{dip}\sin\theta}{\cos\theta(1+\cos\theta)} \end{aligned}. \tag{7}$$

From Eqs. 5 and 7, it can be shown that:

$$\begin{aligned} \tfrac{dx}{d\theta} &= -\left(x - \tfrac{l_{dip}\left(1+\cos\theta-\cos^2\theta\right)}{1+\cos\theta}\right)(\tan\theta+\tan\phi) \\ \tfrac{dy}{d\theta} &= \left(y - \tfrac{l_{dip}(1-\cos\theta)}{\sin\theta(1+\cos\theta)}\right)(\cot\theta-\tan\phi) \end{aligned}. \tag{8}$$

The differential equations given in Eq. 8 need to be solved numerically, however we can make some approximations to allow us to gain some insight into the approximate form of the solution. If we assume that $L_{drift} \gg l_{dip}$, then we can neglect the variation in the point of rotation as the deflecting angle of the raster magnet is varied. In this assumption, we obtain the simplified differential equations:

$$\begin{aligned} \tfrac{dx}{d\theta} &= -x(\tan\theta+\tan\phi) \\ \tfrac{dy}{d\theta} &= y(\cot\theta-\tan\phi) \end{aligned}, \tag{9}$$

which can easily be solved and provides the general solution:

$$\begin{aligned} x &= L_{drift}e^{-\theta\tan\phi}\cos\theta \\ y &= L_{drift}e^{-\theta\tan\phi}\sin\theta \end{aligned}, \tag{10}$$

this solution describes the general equation for an exponential spiral, which is a set of curves, including the Golden Spiral, which have the property that for a line passing through the original and intersecting the spiral, the angle of intersection is a constant. We see that when we apply simplifications to Eq. 8, it produces the correct result as expected. Figure 2 shows a diagram of the hide orientation for an angle of incidence of 70° (a) and 0° (b), based on Eq. 10 and assuming that the point of rotation is independent of deflecting angle, which is a reasonable assumption in this case. In both figures, we can see that the angle of incidence remains constant regardless of the deflecting angle of the beam. The blue lines represent the direction of the electron beam, the black lines show the normal to the hide surface, the red line represents the hide and the green areas demonstrate that the angle of incidence remains constant for non-zero angles of incidence.

When $\phi \neq 0$, the angular range of the beam will not be symmetric. We would either have to shift the midpoint of the hide transversely, or apply a DC offset current to the scanning magnet to shift the range of the angles. In practice, the latter option is likely to be the preferred solution.

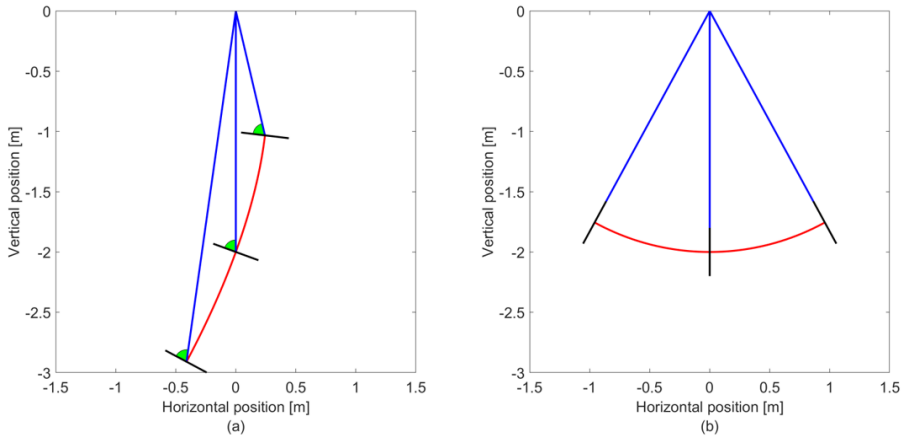

Figure 2. Hide orientation for an angle of incidence of 70° (a) and 0° (b).

So far we have considered the case where the hide is curved in the deflecting plane of the beam in order to ensure that the angle of incidence remains constant. We could also imagine inclining the plane of the hide as it passes through the electron beam, however we would still need to ensure that the angle of incidence in the deflecting plane is zero to ensure we have the angle of incidence we expect; thus we would need to solve Eq. 8 for $\phi = 0$.

2.2. Design of the rastering scheme

The rastering scheme needs to be able to ensure that the beam is swept over the surface of the hide in a uniform manner. For this, there are several key considerations we need to take into account. Firstly, the beam should scan over the surface of the hide at a constant speed, which means that we need to determine how the sweeping speed of the beam depends on deflecting angle. Secondly, we need to consider what raster pattern will ensure a uniform dose distribution.

To determine the speed of the beam as it sweeps across the surface of the hide, we need to determine $\frac{ds}{dt}$, where s is the arc length along the curve describing the hide. The arc length for a curve is given as:

$$s = \int_{x_0}^{x_1} \sqrt{1 + \left(\frac{dy}{dx}\right)^2}\, dx. \tag{11}$$

From Eq. 5, we know $\frac{dy}{dx}$ in terms of the angle of incidence and the magnetic deflecting angle, thus:

$$s = \int_{x_0}^{x_1} \frac{dx}{sin(\theta + \phi)}. \tag{12}$$

Furthermore, we also have an expression relating dx to $d\theta$ from Eq. 8:

$$s = \frac{l_{dip}}{\cos\phi} \int \left(\frac{1}{\cos\theta} - \frac{\cos\theta}{1+\cos\theta}\right) d\theta - \frac{1}{\cos\phi} \int \frac{x}{\cos\theta} d\theta. \tag{13}$$

Due to the fact that Eq. 8 describes an inseparable set of differential equations, it needs to be solved numerically. However, if we use the approximated results from Eq. 10, we can solve this as a simplified form:

$$s = \begin{cases} L_{drift}(\theta - \theta_0), & \text{if } \phi = 0 \\ \frac{L_{drift}}{\sin\phi}\left(e^{-\theta\tan\phi} - e^{-\theta_0\tan\phi}\right), & \text{otherwise} \end{cases}. \tag{14}$$

In Eq. 14, θ_0 is taken to be the deflection angle required to direct the beam to one end of the hide and θ is the angle of some arbitary point on the hide surface. We can use Eq. 13 or 14 to determine the speed of the beam as a function of deflection angle. Eqs. 15 and 16 show equations for the scanning rate of the raster magnet for the exact solution and where $l_{dip} \ll L_{drift}$ respectively. v_{scan} is the scanning speed of the beam on the surface of the hide, which is taken to be a constant.

$$\frac{d\theta}{dt} = \frac{v_{scan}\cos\theta\cos\phi(1+\cos\theta)}{l_{dip}(1+\cos\theta-\cos^2\theta)-x(1+\cos\theta)}. \tag{15}$$

$$\frac{d\theta}{dt} = -\frac{v_{scan}\cos\phi}{L_{drift}}e^{\theta\tan\phi}. \tag{16}$$

From now on, we will assume that $l_{dip} \ll L_{drift}$ as we are able to analyse this case. In a real system, we would expect L_{drift} ~1-2 m, whereas l_{dip} ~0.1 m, therefore, this assumption is valid in this situation. We see that in order to obtain a constant scanning speed, $\frac{d\theta}{dt}$ must vary exponentially with angle, although when $\phi = 0$, the curve becomes a circular arc and $\frac{d\theta}{dt}$ is constant. Given that we want the midpoint of the hide to coincide with the beam when $\theta = 0$ for all values of ϕ, we can define the corresponding range of deflecting angles as:

$$\ln\left(\frac{2L_{drift}}{2L_{drift}+W_{hide}\sin\phi}\right)\cot\phi \leq \theta \leq \ln\left(\frac{2L_{drift}}{2L_{drift}-W_{hide}\sin\phi}\right)\cot\phi. \tag{17}$$

Where W_{hide} is the width of the hide; however in practice it is likely that the beam would be swept slightly further than the width of the hide. If $\phi = 0$, the general form of the integral breakdown as $\int e^{ax}dx \neq \frac{e^{ax}}{a}$ if $a = 0$. So in this case, the range of angles becomes $-\frac{W_{hide}}{2L_{drift}} \leq \theta \leq \frac{W_{hide}}{2L_{drift}}$. From Eq. 17, we can also place some constraints on the geometry of the system. Firstly $\phi < \frac{\pi}{2}$, and we also obtain the condition that $\sin\phi < \frac{2L_{drift}}{W_{hide}}$, if not, the upper bound on deflecting angle becomes complex, which is unphysical.

From Eq. 16, we can solve for $\theta(t)$ and we obtain:

$$\theta(t) = \begin{cases} -\frac{v_{scan}t}{L_{drift}}, & \text{if } \phi = 0 \\ -\ln\left(1+\frac{v_{scan}\sin\phi}{L_{drift}}t\right)\cot\phi, & \text{otherwise} \end{cases}. \tag{18}$$

The negative sign in Eq. 18 is due to the fact that in our definition, a positive angular deflection corresponds to a negative transverse position. This equation defines the required deflection as a function of time in order to sweep across the surface of the hide at a constant rate. In addition to this, we need to take into account the fact that the hide is also moving longitudinally as the beam is being swept across it. As such, we need to give a deflection in the longitudinal direction as well to account for this motion. Furthermore, we need to ensure that the raster pattern forms a closed cycle.

There are an infinite number of choices for the magnetic rastering scheme, but we will consider the scheme which minimises the rate of change of magnetic field for the longitudinal raster magnet. For the remainder of this paper, we will refer to the x-direction as the direction across the width of the hide and the z-direction as the direction of motion. Figure 3 shows a simplified diagram of the raster pattern on the surface of the hide that we need to achieve. The spacing between the horizontal lines is referred to as the pitch, l_{pitch}.

We also need to consider the constraints on the width of the pitch, which will clearly depend on the beam size, σ_{beam}. If we assume that the beam profile is approximately Gaussian, then as we can see from Figure 4, we require that $l_{pitch} \leq \sigma_{beam}$.

For the longitudinal raster magnet, it can be relatively easily shown that the dependence on z with respect to deflection angle is given as:

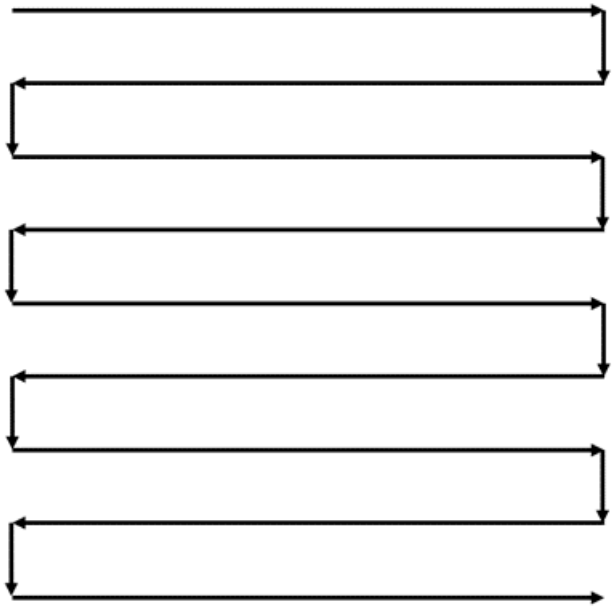

Figure 3. Simplified diagram of the raster pattern required on the surface of the hide.

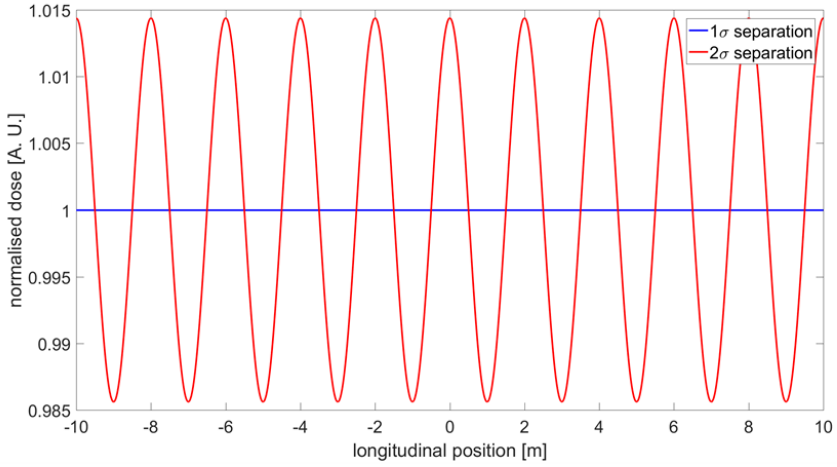

Figure 4. Comparison of surface dose distribution, assuming a Gaussian beam of transverse rms beam size, σ_{beam}, where the pitch width, l_{pitch} is $1\sigma_{beam}$ and $2\sigma_{beam}$.

$$z = \left(L_{drift} e^{-\theta_x \tan\phi} + L_{extra}\right) \tan\theta_z. \tag{19}$$

Note that we have now changed our previous definition of θ to θ_x and the deflecting angle in z is θ_z. L_{extra} is the additional distance that the longitudinal raster magnet is away from the hide relative compared to the horizontal raster magnet; it should be noted that L_{extra} can be negative if the longitudinal raster magnet is downstream of the horizontal raster magnet. In this paper, we will neglect L_{extra} as it is assumed to be small. Given that once again, we want the beam to move in z at a constant speed, which is equal to the speed that the hide moves along the conveyor, which is v_{hide}. We can show that the longitudinal deflection angle as a function of time is given as:

$$\theta_z = \tan^{-1}\left(\frac{v_{hide} t}{\left(L_{drift} + L_{extra}\right) + v_{scan} t \sin\phi}\right) \approx \tan^{-1}\left(\frac{v_{hide} t}{L_{drift} + v_{scan} t \sin\phi}\right). \tag{20}$$

We have now defined the required time dependence of the horizontal and longitudinal raster magnets, however in order to complete a cycle, we need to consider the beam at the edges of the hide, such that the beam spot shifts by one pitch length relative to the hide before scanning across again. To consider the scans from left to right and right to left, v_{scan} simply switches sign. To provide time for the longitudinal raster to shift down one raster, we need to include an overshoot region beyond the end of the hide width. This overshoot region also prevents us delivering an excessive dose to the edge of the hide. The width of this overshoot is somewhat arbitrary, however it is sensible to ensure that it is at least 5-6 RMS beam sizes away from the edge of the hide to avoid excessive dose deposition on the edge of the hide. In order for this scheme to work and to provide a closed raster scheme which provides uniform dose distribution to the surface of the hide, we require:

$$\frac{L_{hide}}{\tau_{hide}} \leq v_{hide} \leq \frac{\sigma_{beam} v_{scan}}{W_{hide} + 2W_{over}}. \tag{21}$$

Where τ_{hide} is the average time to irradiate one hide, L_{hide} is the length of the hide, and W_{over} is the width of the overshoot region. It should be noted that the faster we make v_{hide}, the higher the required raster frequency, which creates challenges on how to vary the magnetic field fast enough. However we need to ensure that v_{hide} is fast enough to produce the required leather throughput to compete with conventional techniques. While a conventional process is a batch process, it typically tans approximately 1 hide every 90 - 360 seconds. In order to minimise the raster frequency, while ensuring that the hide is irradiated within τ_{hide}, we require that Eq. 21 is an equality. Which gives us:

$$v_{scan} = \frac{W_{hide}(W_{hide} + 2W_{over})}{\sigma_{beam} \tau_{hide}}. \tag{22}$$

If we define the beam momentum in MeV/c, then the required magnetic field for a raster magnet is given as:

$$B = 3.3356 \times 10^{-3} \frac{p \sin\theta}{l_{dip}}. \tag{23}$$

Based on all the information we now have, we can fully define the magnetic raster scheme as long as we know the hide width, beam size, overshoot width, tanning time and beam momentum. For this particular application, Table 1 shows the assumed system parameters.

Based on the stated design parameters, Figure 5 shows the magnetic fields for the horizontal (x-direction) and longitudinal (z-direction) raster magnets in the rest frame and the resulting raster pattern as seen on the surface of the hide. In Figure 5(b), the red lines represent the edge of the hide width, to show the overshoot region. Figures 5(c) and (d)

Table 1: Table of the assumed system design parameters for the proposed raster scheme.

Parameter	Value
W_{hide}	2 m
σ_{beam}	1 cm
W_{over}	5 cm
τ_{hide}	90 s
p	3.46 MeV/c
v_{scan}	4.67 m/s
v_{hide}	0.022 m/s
l_{dip}, x/z	20 cm / 5 cm
L_{drift}	2 m
l_{pitch}	1 cm
Raster frequency	1.11 Hz

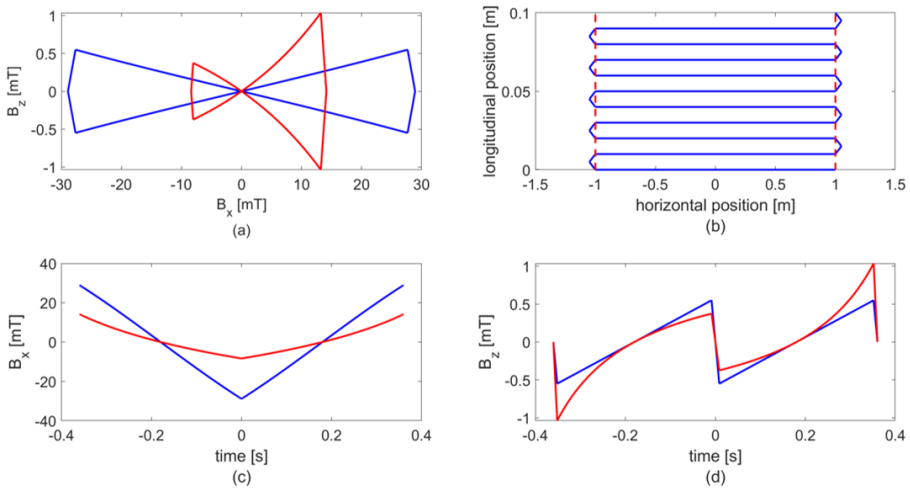

Figure 5. Raster pattern for an angle of incidence of 0° (blue) and 70° (red) in the rest frame (a), the projected raster pattern on the surface of the hide (b), B_x (c) and B_z (d) vs. time. In (b), the raster pattern projected on the surface of the hide is the same for all angles of incidence. The dashed red lines represent the edge of the hide to highlight the overshoot regions.

show B_x and B_z as a function of time. Note that for this particular choice of raster pattern, the longitudinal raster magnet oscillates at double the frequency of the horizontal raster. In doing so, the raster pattern in the rest frame forms a figure of 8 pattern and this set up allows us the minimise the range of movement in the longitudinal direction. We could, however, design a raster pattern that would appear as a triangle in the rest frame, but this would double the dynamic range for the longitudinal raster magnet.

3. Simulation studies

3.1. Irradiation and Energy Deposition

In this section, we present simulation results where we have studied the beam energy and beam delivery requirements in order to achieve uniform depth dose distribution in the hide by using G4beamline [12], which is based on GEANT4 [13]. Geant4 is a freely distributed toolkit under open software licence and based on C++ using Monte Carlo method for the simulating of particle interaction with matter. G4beamline is particle tracking simulates both accelerator beamlines and particle interaction with the matter. The wet hides have an assumed density approximately 3 times that of water and thickness around 8 mm. Therefore, in radiation deposition simulations the hide is approximated/replaced by using water with 2.5 cm depth.

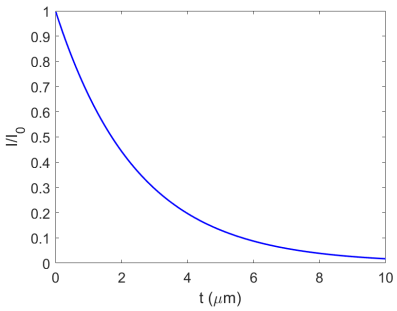

Figure 6. Attenuation of 1 keV X-ray in the liquid water.

3.1.1. Physics Model

The physics list used in our simulations is FTFP_BERT_LIV. FTFP_BERT is the current Geant4 default and is good for most HEP (High Energy Physics) processes. The FTFP_BERT_LIV uses a set of EM (Electromagnetic) processes with accurate simulation of gamma and charged particle transport by using Livermore set of models [14]. The default energy threshold limit of 990 eV is used. The physics processes include: photoelectric effect; Compton scattering; Rayleigh scattering; gamma conversion; ionization; and bremsstrahlung.

We can estimate the average distance traveled of photons in the matter by using equation

$$\frac{I}{I_0} = e^{-\frac{\mu}{\rho}x} \tag{24}$$

where I_0 is the incident intensity, I is the intensity at mass thickness x, $\frac{\mu}{\rho}$ is the mass attenuation coefficient [15] of the target. The mass thickness is given by

$$x = \rho t \tag{25}$$

with ρ being the density and t being the thickness of the material X-ray traveling. The $\frac{\mu}{\rho} = 4.078 \times 10^3$ cm^2/g for the 1 keV X-rays in the water. The attenuation of 1 keV X-ray in the liquid water can be shown as in Fig. 6. The intensity of the 1 keV X-rays are reduced to less than 2% in the 10 μm of water, which indicates the error introduced by implementing 1 keV cut-off energy in the simulation would be on the order of microns. Such an error is negligible as the water thickness in consideration in our study is 4 orders of magnitude larger. As the electron interacts with more strongly than photon as it carry charge, the the error introduced by electrons would be even smaller than photons.

We also tested Penelope set of models by using physics list FTFP_BERT_PEN. They generated similar depth-dose curve as shown in the Figure 7, which closely resembles the results given in the Ref [16].

3.1.2. Double-sided irradiation

The energy deposited by the electron beam at a certain depth, known as the depth-dose curve or dose deposition curve, is energy dependent, as shown in the Figure 8, where we consider the case where the hide is irradiated from one side (a) or both sides (b). The choice of single- or double-sided irradiation depends on several key factors and throughout this section we shall explore both possibilities.

We shall start by looking at double-sided irradiation as this requires a lower energy beam and has a higher energy efficiency than single-sided irradiation, as almost no radiation completely penetrates the entire thickness of the hide. However, assuming the hide density and thickness stated earlier, a beam energy below 2.5 MeV fails to penetrate to the central region of the hide and for beam energies below 3.5 MeV, the peak dose deposition occurs before the central region.

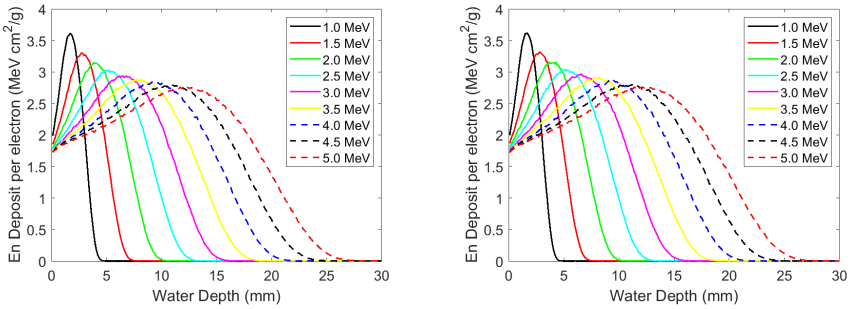

Figure 7. Depth-dose curves generated by different energies of electrons in the water in simulation by using (a) Livermore and (b) Penelope set of models.

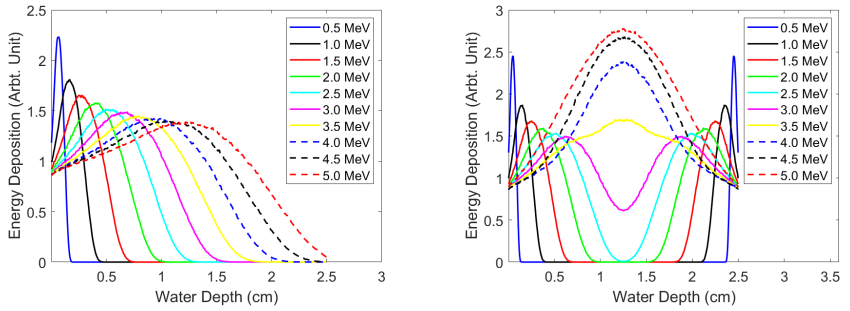

Figure 8. Energy deposition vs. water depth for different beam energies when irradiated from one side (a) and both sides (b) for an angle of incidence of 0°.

In order to achieve a uniform dose distribution through the hide, beams with different dose deposition curves are required. This can be achieved in several ways, but the two methods we will consider are where the beam energy is modulated (or the energy spectrum tailored) and where the angle of incidence is varied. As we shall see further on, varying the beam energy is qualitatively equivalent to varying the angle of incidence. We shall define the dose deviation, D_d, as the percentage variable in dose distribution along the depth of water:

$$D_d = \left(\frac{D}{D_{ave}} - 1 \right) \times 100\%, \tag{26}$$

where D is the dose along the depth and D_{ave} being the average of D. By using the dose deposition curves in Figure 8, we applied a least-squares algorithm to obtain the required energy spectrum of the beam as shown in Figure 9(a), which will provide the uniform dose distribution shown in Figure 9(b).

Unfortunately, the energy spectrum determined from the least-squares method is practically impossible to achieve. Due the the required dipole magnets to direct the beam, we expect that the maximum tolerable energy spread of the beam would be approximately 1%. An excessive energy spread would result in an energy modulation of the beam across the surface of the hide, which would impact the dose uniformity.

Figure 10 shows another solution, whereby rather than attempted to produce a complicated energy spectrum for a single pass irradiation, we consider the possibility where the hide is irradiated over multiple passes and on each pass, the beam energy and corresponding magnet strengths are varied to produce a relatively flat dose deposition curve (b) from a series of beams with different energies and intensities (a). This approach greatly simplifies the set up, at the expense of requiring multiple passes of the electron beam. When operating the system in multi-pass mode, we would need to consider factors such

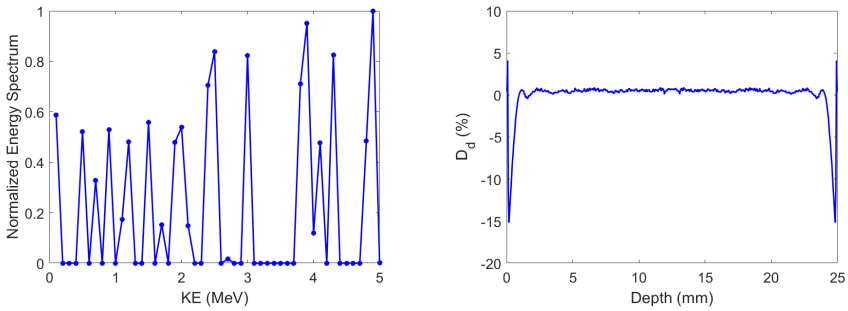

Figure 9. The energy spectrum (a) and dose deviation (b) obtained by a least-squares method to provide a uniform depth-dose curve.

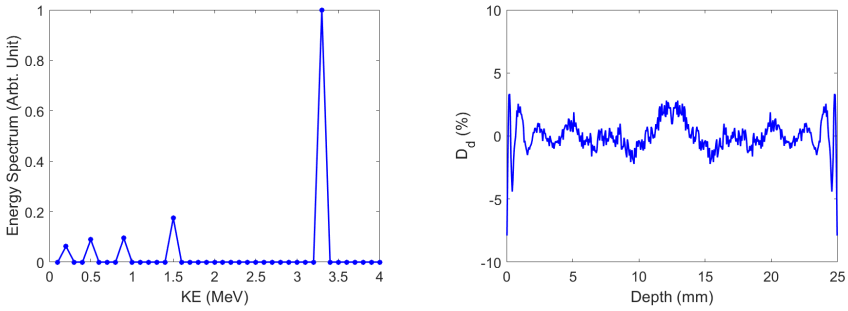

Figure 10. Energy spectrum for multi-pass, multi-energy irradiation of the hide (a) and the resulting dose deviation (b). The spectrum is obtained by using least-squares algorithm and limiting combination to 5 mono-energetic beams.

as the raster magnet scanning rate, although this is not perceived to be a major issue as a raster frequency of $\sim$ 100 Hz is achievable and multi-pass irradiation would require a raster frequency of approximately 10 Hz. It should also be noted that this approach produces a better dose uniformity near the surface when compared to Figure 9.

3.1.3. Dependence on angle of incidence

In the previous subsection, we noted that achieving a uniform dose distribution through the thickness of the hide would be practically impossible as a majority of the low-energy particles would be excessively scattered in the dipole magnets, and generation of such a spectrum would not be possible with a single accelerator. Furthermore, it should be noted that for multi-pass operation, it would be extremely challenging to repeatably produce beams below $\sim$1 MeV with a linear accelerator. Instead, this system would likely require a low-energy accelerator ($>$ 1 MeV) and a high-energy linear accelerator; which would likely drive up the cost of such a system. Another alternative is to consider a multi-pass system, where the angle of incidence of the beam onto the surface of the hide is varied on each pass; while maintaining a constant beam energy, or requiring a much smaller range of energies. When electrons collide with the hide at an angle, more dose is deposited nearer the surface than for head-on irradiation; as shown in the Figure 11. In this case, we are assuming that the hide is irradiated from both sides to create a symmetric dose distribution pattern. This can be achieved by irradiating each side of the hide on separate passes. As a result, the effect of a non-zero angle of incidence is qualitatively similar to irradiating the hide with a lower energy beam, as can be seen in the Figure 12.

As previously stated, we can combine dose deposition curves at different energies and different angles to generated a more uniform dose profile as shown in the Figure 13, where we have assumed that the hide is irradiated from both sides over a total of four passes.

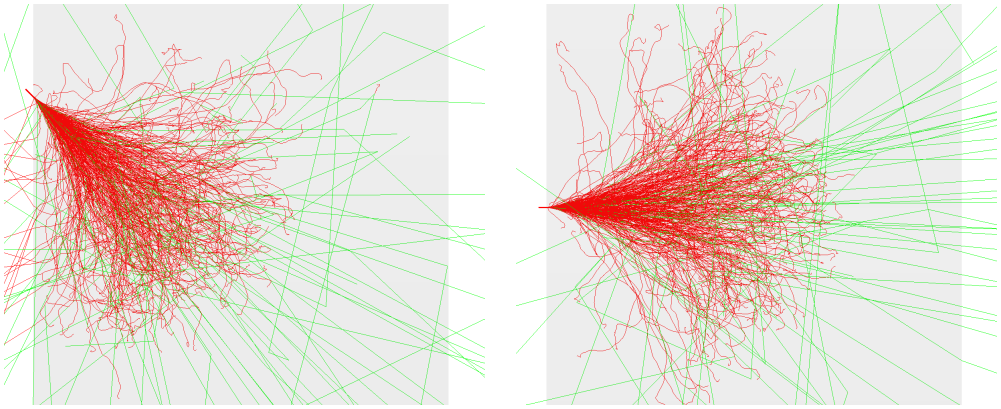

(a) (b)

Figure 11. Irradiation with 3.5 MeV at (a) 0° and (b) 45° angle beams. The red/green lines are the trajectories of electrons/photons. The grey color is 2.5 cm thick (from left to right) water.

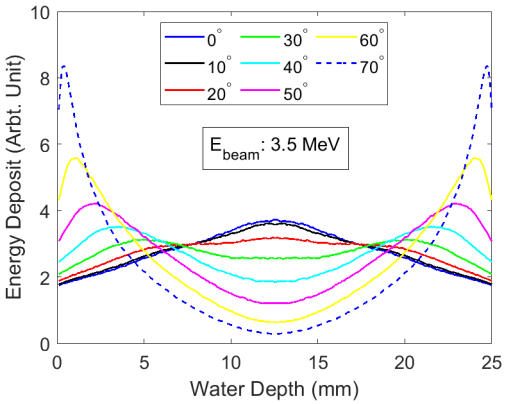

Figure 12. Depth-dose curves for a 3.5 MeV beam with a varying angle of incidence.

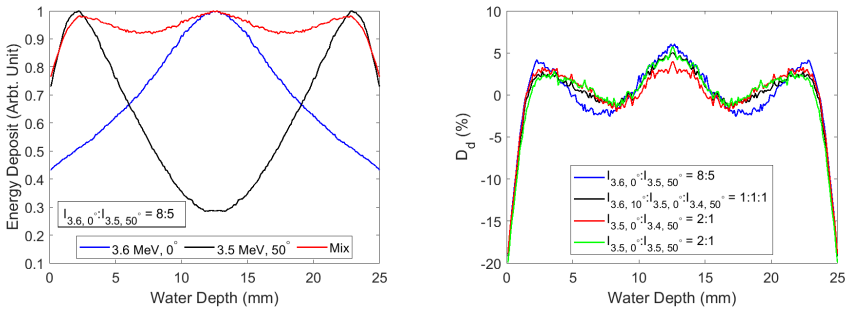

Figure 13. Combined depth-dose curves for a 3.5 MeV beam with an angle of incidence of 50° and a 3.6 MeV beam with an angle of incidence of 0° (a) and a comparison of dose deposition curves for different combinations of beam energy and angles of incidence (b).

Figure 13(a) shows one example case where the dose deposition curves are added together for beams with different energies and angles of incidence (blue and black curves) and the combined dose distribution curve is shown in red. Figure 13(b) shows a comparison of the optimal dose deposition curve for different sets of parameters, where the beam energy and angle of incidence are varied. In the legend, $I_{x,y}$, represents the normalised intensity for a beam of energy, x MeV, and an angle of incidence of $y°$. In this plot, it should be noted that we have limited the maximum angle of incidence to 50°. From plot (b), it should be noted that the dose deposition curves are all similar, but the simplest configuration is the green curve because the beam energy remains constant and only the angle of incidence is varied.

The beam energy can be modulated in several ways. The simplest solution is to vary the linac accelerating gradient and dipole field strengths to achieve the required beam energies. Alternatively, another more complicated approach is to apply the beam energies in a single pass by extracting portions of the beam at different energies with the use of septum magnets [11]. The blue, black and green curves show the relative energy deposition from a series of mono-energy beams at indicated angles and beam energies. The red lines are the energy deposited by the mixture of these beams at the indicated mix ratios.

Large angles of incidence can be used to improve the dose uniformity near the surface, as shown in the Figure 14. The large angle of 70° deposits most of its energy near the surface; similar to the dose deposition from a low energy beam. We can define the depth dose uniformity U_{dd} as

$$U_{dd} = \frac{D_{max} - D_{min}}{D_{ave}}, \tag{27}$$

where, D_{max}, D_{min}, and D_{ave} are the maximum, minimum, and average dose deposition respectively. U_{dd} for Figure 14 is 8.6%. Another similar parameter we can use, which takes into account the actual beam distribution, is the normalised RMS dose deposition, σ_{D_r}, which is the ratio of the standard deviation of the depth dose, σ_D, and the average depth dose, $\sigma_{D_{ave}}$, which can be written as:

$$\sigma_{D_r} = \frac{\sigma_D}{D_{ave}}, \tag{28}$$

where for Figure 14, σ_{D_r} = 1.7%.

3.1.4. Single-sided irradiation

In addition to irradiating the hides from both sides, we can consider a slightly simpler set up where the hides are irradiated from just one side. In doing so, we would need to use higher energy beams, and a significant portion of the beam energy would penetrate though the hide, reducing the energy efficiency of the entire process. The depth-dose curves are shown for the 6−10 MeV beams for an angle of incidence of 0° (Figure 15). We see the

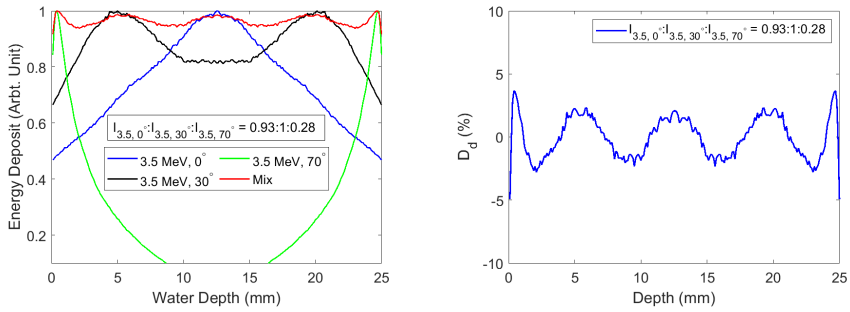

Figure 14. Dose deposition curves for different angles of incidence (a) and corresponding dose deviation (b) of 3.5 MeV beam.

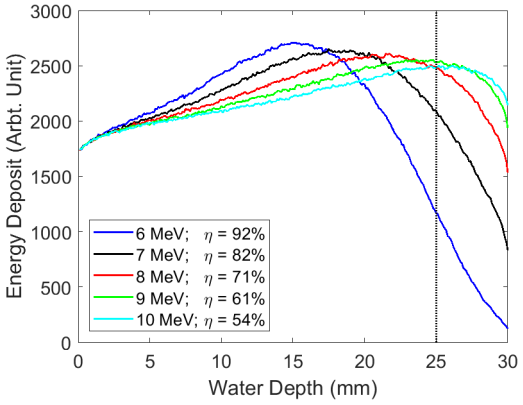

Figure 15. Single sided irradiation with high energy beams.

beam energy needs to be at least 8 MeV to achieve good dose deposition on the far side of the hide.

However, the key disadvantage with single-sided irradiation is that a significant portion of beam energy passes completely through the hide, resulting in a reduced energy efficiency when compared to double-sided irradiation. The irradiation efficiency η can be defined as

$$\eta = \frac{P_{dep}}{P_0}, \tag{29}$$

where P_{dep} and P_0 are the deposited and incident beam power, respectively. As the beam energy increases, some of the electrons will penetrate though 25 mm water and the energy is not used for the tanning process. From Figure 15, the irradiation efficiencies for 8 MeV and 9-MeV beams are 71% and 61% respectively.

Figure 16 shows the dose deposition curves for an 8 MeV beam (a) and a 9 MeV beam (b) and the dose deviation is shown for the 8 MeV (c) and 9 MeV (d) beams respectively. Qualitatively, these plots are similar, but the higher penetration from the 9 MeV beam improves the dose deposition on the far side of the hide.

Figure 17 shows the combined dose deviation curves from Figures 14 and 16 to show a comparision between single- and double-sided irradiation. As we can see, both techniques have similarly flat dose depositions, but single-sided irradiation is slightly flatter and also requires fewer passes to achieve a similar level of flatness.

Single-sided irradiation would require much higher beam energies than for double-sided irradiation. Furthermore, the reduced irradiation efficiency for single-sided irradiation means that a significant amount of dose is deposited in the conveyor system and supports, resulting in increased radiation and reducing the lifetime of components. How-

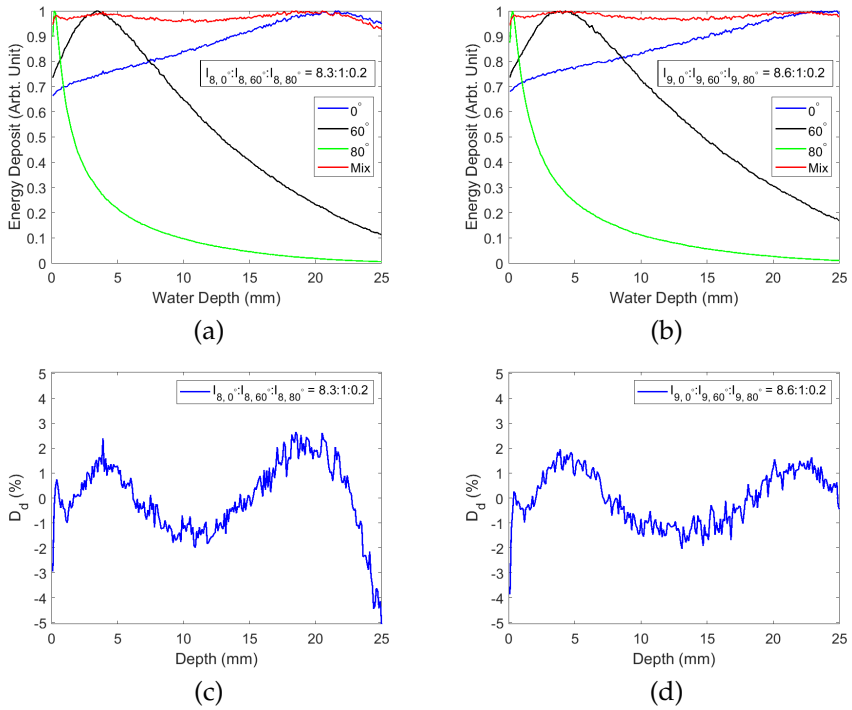

Figure 16. Single-sided irradiation by combining beams with different angles of incidence for (a) 8 MeV and (b) 9 MeV beams. Dose deviation for (c) 8 MeV and (d) 9 MeV beams.

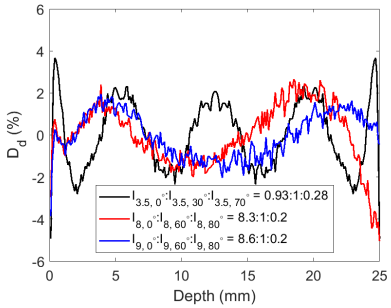

Figure 17. Comparison of dose deviation of single- and double-sided irradiation.

ever, as we can see from the plots and table, single-sided irradiation significantly improves dose flatness, which in turn will improve tanning uniformity. The overall impact on capital and running costs of the two systems as well as system complexity and reliability will be considered in future studies.

4. Conclusions

In this paper, we have presented a design study for an electron accelerator in order to irradiate hides for a novel leather tanning process. As discussed in the introduction, ensuring that we can achieve a uniform dose distribution throughout the volume of the hide is essential for effective tanning.

In Section 2, we present a design study for a magnetic rastering scheme in order to scan the beam over the surface of the hide as it is passed through the beam on a conveyer system, such that the surface dose distribution is uniform. We derived the differential equations that govern the rastering scheme and solve these with appropriate simplifications in order to determine the the rastering scheme. We also show that we can successfully vary the angle of incidence of the beam, while still maintaining a uniform surface dose distribution.

Table 2: Single and two sided slant irritation results.

irradiated scheme beam energy (MeV)	double-sided 3.5	single-sided 8	single-sided 9
η	96.6%	73.1%	64.6%
U_{dd}	8.5%	7.7%	5.8%
σ_{D_r}	1.6%	1.5%	1.1%

In Section 3, we undertake dose deposition simulations using G4BeamLine in order to determine the energy spectrum of the beam required to achieve a uniform depth-dose curve. Initially, we consider a single pass, with zero angle of incidence (so the beam in perpendicular to the surface of the hide). In this case, we concluded that the energy spectrum would not be possible to achieve and that the lower energy particles would be lost by the deflecting magnets after the linac. We next considered a multi-pass system, where the beam is quasi-monoenergetic and a different beam energy is used on each pass and determined that this can produce acceptable dose uniformity. When then considered that we vary the angle of incidence instead of the beam energy and determined that this is qualitatively equivalent to varying the energy. We considered single and double-sided irradiation and found that single-sided irradiation is preferable for overall energy efficiency, but double-sided irradiation provides better dose uniformity. Hence the choice of single- or double-sided irradiation would ultimately depend on other parameters, such as available space, beam energy and current as well as the required time to irradiate each hide.

5. Acknowledgements

The research in this paper was funded by STFC with Grant Nos. ST/S002189/1 and ST/P002056/1 (Cockcroft Institute Core Grant). Furthermore, we would like to express our gratitude to Elizabeth Mullis for supporting this work and helping to establish collaborative ties with academic institutes and industrial partners.

References

1. O. Bruning et al., LHC Design Report, CERN Yellow Reports: Monographs, 2004, https://cds.cern.ch/record/782076, http://dx.doi.org/10.5170/CERN-2004-003-V-1
2. L. Linssen et al., Physics and Detectors at CLIC: CLIC Conceptual Design Report, 2012, http://dx.doi.org/10.5170/CERN-2012-003
3. C. Adolphsen et al., The International Linear Collider Technical Design Report - Volume 3.II: Accelerator Baseline Design, 2013, ILC-REPORT-2013-040, https://arxiv.org/abs/1306.6328
4. UNIDO's leather panel, Case study: leather industry parks, 2017, https://leatherpanel.org/content/case-study-leather-industry-parks-planning-implementation-benefits-challenges-and-experience
5. M. Mwinyihija, Ecotoxicological Diagnosis of the Tanning Industry, (2010), DOI: 10.1007/978-1-4419-6266-9, https://www.semanticscholar.org/paper/Ecotoxicological-Diagnosis-in-the-Tanning-Industry-Mwinyihija/3395884c77441d2641dc51b83fcd58fa40ee45ce
6. A. Blackman, Adoption of Clean Leather-Tanning Technologies in Mexico, 10881, Resources for the Future, DOI: 10.22004/ag.econ.10881, https://ideas.repec.org/p/ags/rffdps/10881.html, (2005)
7. RCRA in Focus - Leather Manufacturing, US Environmental Protection Agency, (2005), https://www.epa.gov/sites/production/files/2015-01/documents/k00002.pdf
8. EU legislation regarding the leather industry, https://ec.europa.eu/growth/sectors/fashion/leather/legislation_en
9. R. Apsimon, T. Junginger, R. Seviour, Process for tanning animal hide Inventors: , UK patent application GB1914917.8
10. L.J. Lindgren, A. Sandell, M. Eriksson, Fast kicker magnet system, Nuclear Instruments and Methods in Physics Research, Volume 214, Issues 2–3, 1983, Pages 175-178, ISSN 0167-5087, https://doi.org/10.1016/0167-5087(83)90583-5

11. M. Barnes et al., Injection and extraction magnets: septa, in Proceedings of the CAS-CERN Accelerator School: Magnets, Bruges, Belgium, 16-25 June 2009, edited by D. Brandt, CERN-2010-004 (CERN, Geneva, 2010), http://dx.doi.org/10.5170/CERN-2010-004.167
12. Muons, Inc., http://www.muonsinternal.com/muons3/G4beamline, 2015-11-02.
13. S. Agostinelli *et al*. Geant4—a simulation toolkit, Nuclear Instruments and Methods in Physics Research Section A: Accelerators, Spectrometers, Detectors and Associated Equipment, Volume 506, Issue 3, 2003, Pages 250-303, ISSN 0168-9002, https://doi.org/10.1016/S0168-9002(03)01368-8
14. Geant4 Physics Rerference Manual, Release 10.7, Geant4 Collaboration, Rev5.0: December 4th, 2020.
15. X-Ray Mass Attenuation Coefficients, NIST Standard Reference Database 126, Last Update to Data Content: July 2004, https://dx.doi.org/10.18434/T4D01F
16. INTERNATIONAL ORGANIZATION FOR STANDARDIZATION, ISO/ASTM 51649:2002 Standard Practice for Dosimetry in an Electron Beam Facility for Radiation Processing at Energies Between 300 keV and 25 MeV, ISO, Geneva (2002).